

Influence of Secondary Factors of Spindle Geometry on the Dynamic Stability in End-milling Operation

Jakeer Hussain Shaik*, J. Srinivas

Department of Mechanical Engineering, National Institute of Technology, Rourkela, India

*Corresponding author: jakeershaik786@yahoo.co.in

Received June 03, 2014; Revised June 09, 2014; Accepted June 15, 2014

Abstract Chatter is a issue of uncertainty in the metal reducing procedure. The trend is characterized by aggressive oscillations, noisy sound and low quality of surface finish. Chatter causes a reduction of the life of the device and affects the efficiency by disrupting the regular functioning of the machining procedure. This paper presents a coupled model of high-speed end-mill spindle system by considering the dynamics of angular contact ball bearings and cutting forces. Initially, the spindle device is examined by considering the gyroscopic and centrifugal terms using Timoshenko beam theory. Hertz bearing contact forces considered at front and rear side ends of the spindle. Frequency response functions at the tool-tip are obtained from the dynamic spindle model. In the second phase, solid model of the system is developed and its dynamic response is obtained from three dimensional finite element analysis. After, verification of the outcomes with beam theory concept, the stability lobes are plotted from the tool-tip frequency response (FRF). Later parametric analysis are conducted for different tool-overhang measures, bearing span values and helix angle of the cutting tool conditions to effectively plot the stability lobes for the spindle system.

Keywords: spindle dynamics, stability, bearing contact forces, timoshenko beam element, solid modeling, parametric analysis

Cite This Article: Jakeer Hussain Shaik, and J. Srinivas, "Influence of Secondary Factors of Spindle Geometry on the Dynamic Stability in End-milling Operation." *Journal of Mechanical Design and Vibration*, vol. 2, no. 2 (2014): 35-46. doi: 10.12691/jmdv-2-2-1.

1. Introduction

High speed machining technology has been widely used in automotive, aerospace, die making, electronics and many other industries to increase productivity and reduce production costs. This technology is mainly limited by the performance of the spindle which has a significant influence on the machining accuracy. Self-excited vibrations of the tool resulting-in unstable cutting process which leads to the chatter on the work surface and it reduces the productivity. At large rates of material removal, tool chatter creates the unavoidable flexibility between the cutting tool and the work piece; if it is uncontrolled the chatter causes a rough surface finish and dimensional inaccuracy of the work piece along with unacceptable loud noise levels and accelerated tool wear. The chatter stability of the tool is dependent on the dynamic behavior of the spindle system, which is often expressed as the FRF at the tool tip. In other words, tool-tip FRF is a key variable in determination of stability limit given by Altintas and Budak (1995). The objective of the design engineer is to predict the cutting performances of the spindle during the design stage by relying on engineering model of the process and system dynamics. Early spindle research has focused mainly on static analysis, where as current research is extended to the dynamics for optimal design.

Over the last two decades, numerous approaches have been addressed to elaborate the tool-tip FRF through modeling and experiments. With introduction of receptance coupling substructure analysis by Schmitz and Duncan in early [4]. Later Jun et al. [6] had illustrated the approach to predict the tool point FRFs. Erturk et al. [8] presented analytical models to obtain the tool-tip FRF. Faassen et al. [9] predicted chatter stability lobes of high speed milling on the basis of experimental FRFs at different spindle speeds. Abele and Fiedler [10] introduced a sub-space-state-space-identification method to measure and calculate the dynamic behavior of spindle-tool systems during high speed machining, consequently, stability lobe diagrams were determined based on the identified FRFs. Zaghbani and Songmene [11] used operational modal analysis to estimate the machine tool dynamic parameters during high machining operations, and the dynamic stability lobes were calculated using the extracted modal parameters. The experimental method is used to identify speed-varying dynamics of spindles in the above works, which is direct and feasible. However, it is time-consuming to repeat the modal tests for every spindle speed and prone to errors. With known details of the spindle geometry, drawbar force, bearing parameters and preload, etc., an alternative method to obtain the dynamic behavior of spindle system is the finite element (FE) method. With the accurate spindle model, the FRFs at the tool tip are simulated and

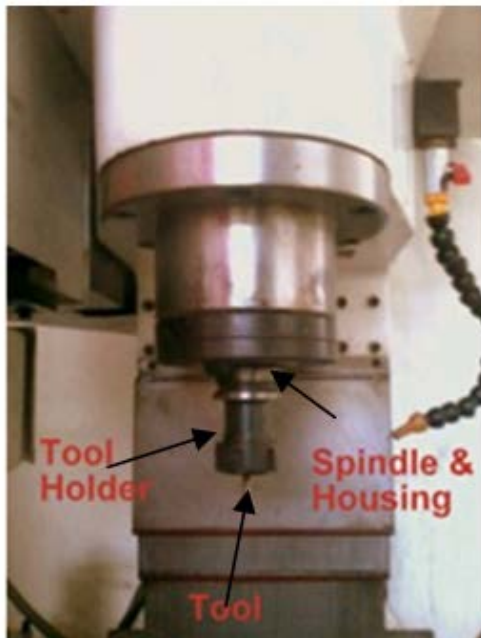
then chatter stability lobes can be predicted. Chen and Wang [12] modeled the integrated spindle-bearing system and they also found that significant errors occurred in predicting stability lobes if the load and speed effects on the shaft/bearing dynamics were neglected. Tian and Hutton [13] considered the gyroscopic effects of the rotating spindle and proposed a chatter model in milling systems. They found that gyroscopic effects reduced the critical axial depth of cut. Xiong et al. [14] developed a new dynamic milling model of a rotating spindle and the gyroscopic effect of the spindle on the stability characteristics of the milling system is investigated. Similarly, Movahhedy and Mosaddegh [15] predicted the chatter in high speed milling including gyroscopic effects on the basis of finite element model of spindle. Gagnol et al. [20] developed a dynamic model of a high-speed spindle system and then proposed a dynamic stability lobe diagram by integrating the speed-dependent FRFs of spindles into analytical approach. Angular contact ball bearings are commonly used in high-speed spindles due to their low-friction properties and ability to withstand external loads in both radial and axial directions. Although the ball bearings appear to be a simple mechanism, their internal geometry is quite complex and often display very complicated nonlinear dynamic behavior. It is obvious that the spindle machining system supported by ball bearings present interesting stability characteristics and nonlinear responses. Several recent studies illustrated the dynamics of high speed spindles under different preload mechanisms and operating speeds.

Present paper describes a coupled model of spindle-bearing system by considering the effects of ball bearing

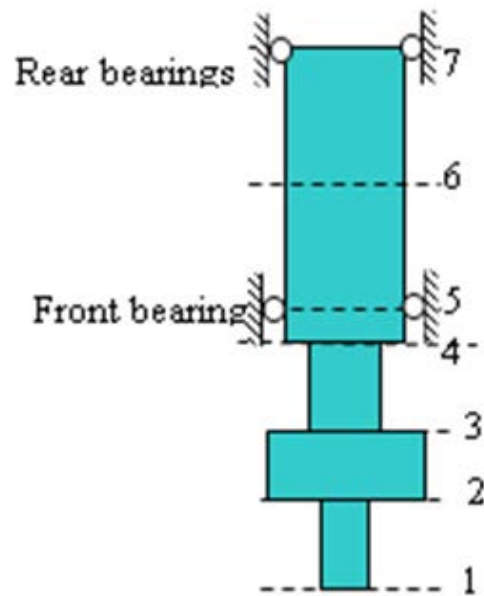
Hertz contact forces on the spindle dynamics. The governing differential equations of motion of spindle system are employed and numerical simulations are carried-out using Timoshenko finite element beam model. Tool-tip FRFs are calculated to plot the stability lobe diagrams for this spindle bearing system using the known depths of radial immersion in high speed end-mill machining process. This spindle system is also modelled as a solid geometry and analysed by using 3-D finite element mesh. Modal and harmonic analyses are conducted to validate the dynamic characteristics of the coupled spindle-tool unit. After ascertaining the realistic model of the spindle unit, some parametric studies are conducted to know the effect of tool-overhang length, helix angle of the cutting tool and different bearing span ratios on the system stability in terms of fundamental natural frequency and average stable depth of cut. The organization of the paper is as follows: section-2 explains the finite element modelling of spindle-bearing unit and section-3 deals with cutting process dynamics and forces during end-milling operation. Results and discussions are presented in section-4.

2. Modeling of Spindle-Bearing System

The typical end-mill spindle system consists of spindle housing carrying spindle shaft on the front and rear bearings along with a tool holder and the tool as shown in Figure 1a. The dynamic behavior of the spindle-tool unit is well established through the modeling of the restricted spindle rotating system on the bearings as shown in Figure 1b.



(a) Schematic of end-mill spindle unit



(b) Equivalent analysis model

Figure 1. Schematic of spindle assembly

The governing equations of motion for the spindle-shaft system based on Timoshenko beam theory are [22,23]:

$$\rho A \frac{d^2 v}{dt^2} - \frac{\partial}{\partial x} \left[k_s A G \left(\frac{\partial v}{\partial x} - \theta_z \right) - P \frac{\partial v}{\partial x} \right] - \Omega^2 \rho A v = F_x \quad (1)$$

$$\rho A \frac{d^2 w}{dt^2} - \frac{\partial}{\partial x} \left[k_s A G \left(\frac{\partial w}{\partial x} + \theta_y \right) - P \frac{\partial w}{\partial x} \right] - \Omega^2 \rho A w = F_y \quad (2)$$

$$\rho I \frac{d^2 \theta_y}{dt^2} + \Omega \rho J \frac{d \theta_z}{dt} - EI \frac{\partial^2 \theta_y}{\partial x^2} + k_s A G \left(\frac{\partial w}{\partial x} + \theta_y \right) = M_x \quad (3)$$

$$\rho I \frac{d^2 \theta_z}{dt^2} - \Omega \rho J \frac{d \theta_y}{dt} - EI \frac{\partial^2 \theta_z}{\partial x^2} - k_s AG \left(\frac{\partial v}{\partial x} - \theta_z \right) = M_y \quad (4)$$

Here, v and w are the bending deformation in two perpendicular directions of the spindle unit. ρA is mass per unit length of spindle shaft, k_s is shear deformation factor, EI is flexural rigidity, AG is shear rigidity of the shaft material, ρJ is polar modulus, F_x and F_y are the components of external forces, M_x and M_y are the components of transverse moments and Ω is the speed of rotation of spindle shaft. A two-node beam element incorporating rotary inertia and shear deformation effects based on Timoshenko beam theory given by Nelson [24] is employed to model the rotating spindle. It has four degrees of freedom per node and the translational, rotational mass matrices, stiffness and gyroscopic matrices of each element are obtained by applying Hamilton's principle. The overall equations in matrix form can be written as:

$$[M]\{\ddot{q}\} + [C]\{\dot{q}\} + ([K] - \Omega^2[M_c])\{q\} = F \quad (5)$$

where $[M]$, $[C]$ and $[K]$ are the assembled mass, viscous damping and stiffness $[K]$ matrices, Ω is speed of rotation, while $[G]$ represents the gyroscopic matrix and the term $\Omega^2[M_c]\{q\}$ indicates the softening effect of spring forces. The front and rear portions of the spindle shaft are supported by the similar angular contact ball bearings. The stiffness behavior of angular contact bearings depend on the applied loads and the bearing layout. Empirical formulae are proposed in literature to evaluate the static radial stiffness of the bearings in terms of axial preload (F_a), ball diameter (D_b), number of balls (N_b) and contact angle of static angular-contact ball bearing (θ) and one such useful expression is presented by Liu et al. [25]:

$$k = 1.77236 \times 10^7 \times (N_b^2 \cdot D_b)^{1/3} \frac{\cos^2 \theta}{\sin^{1/3} \theta} F_a^{1/3} \text{ N/m} \quad (6)$$

Without considering the axial forces and moment loadings of the spindle system, the dynamic problem of the angular contact ball bearing is made as one of the two degrees of freedom model. The local Hertz contact forces and deflection relationships for rolling elements with the inner and outer races may be written as a following set of restoring force components:

$$F_{x1} = -c_{b1} \dot{x}_{b1} - \sum_{i=1}^{N_b} k_{b1} \left(\begin{array}{c} x_{b1} \cos \phi_i \\ + y_{b1} \sin \phi_i - \delta \end{array} \right)^{1.5} \cos \phi_i \quad (7)$$

$$F_{y1} = -c_{b1} \dot{y}_{b1} - \sum_{i=1}^{N_b} k_{b1} (x_{b1} \cos \phi_i + y_{b1} \sin \phi_i - \delta)^{1.5} \sin \phi_i \quad (8)$$

$$F_{x2} = -c_{b2} \dot{x}_{b2} - \sum_{i=1}^{N_b} k_{b2} \left(\begin{array}{c} x_{b2} \cos \phi_i \\ + y_{b2} \sin \phi_i - \delta \end{array} \right)^{1.5} \cos \phi_i \quad (9)$$

$$F_{y2} = -c_{b2} \dot{y}_{b2} - \sum_{i=1}^{N_b} k_{b2} \left(\begin{array}{c} x_{b2} \cos \phi_i \\ + y_{b2} \sin \phi_i - \delta \end{array} \right)^{1.5} \sin \phi_i \quad (10)$$

Here δ refers to the initial clearance of the bearings, N_b is number of balls, x_{b1} and y_{b1} , x_{b2} and y_{b2} are the displacements of mass elements distributed at the front

and rear bearing nodes along x and y directions respectively, k_{b1} and c_{b1} , k_{b2} and c_{b2} are the stiffness and damping of front and rear bearings respectively, the angle $\phi_i = [\Omega r / (R+r)]t + (2\pi / N_b)(i-1)$, (where $i=1, 2, \dots, N_b$) is the angular location of the i^{th} ball. Here the displacement term: $x_b \cos \phi_i + y_b \sin \phi_i - \delta$ is accounted only when it is positive, otherwise it is taken as zero and the bearing races are at loss of contact with bearing balls. The spindle frequency response can be obtained through Fourier transformation of the time-domain response derived by solving Eq. (5) by incorporating the Hertz contact forces at the bearings in the right hand side force vector $\{F\}$. If the bearing stiffness is known, then the FRF consisting of real and imaginary parts can be expressed without time-integration scheme as follows:

$$[H(j\omega)] = [Re(w)] + j[Im(w)] \\ = [-[M]\omega^2 + j\omega[C] - W[G]] + ([K] - W^2[M_c])^{-1} \quad (11)$$

Here, Re and Im are, respectively, the real and imaginary part of the transfer/frequency response functions of the spindle-tool unit model.

3. Dynamics of Cutting Process

The cutting force is chosen as the source signal for chatter because of the availability of well-established mechanistic models for milling. Consider a milling cutter with two degrees of freedom and N_t number of teeth with a zero helix angle as shown in Figure 2. The tool is assumed to be compliant relative to the rigid work piece. The vibration is excited by the summation of cutting force.

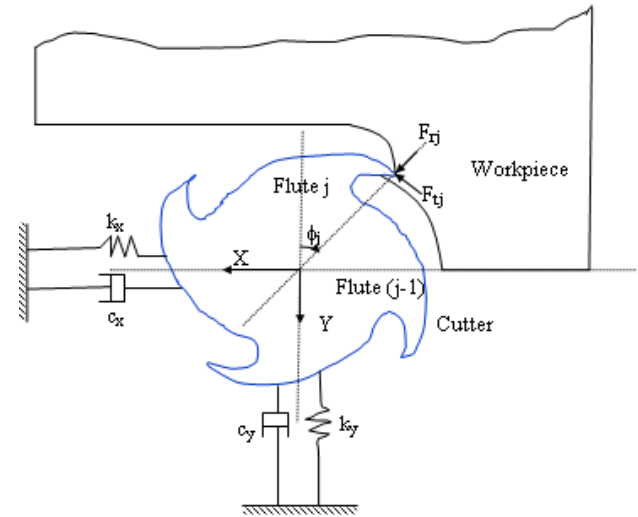


Figure 2. Two-degree of freedom milling model

The cutting forces excite the structure in feed and normal directions, causing dynamic displacements x and y , respectively. If the spindle rotates at an angular speed of Ω (rad/s), the immersion angle vary with time as $\phi_i(t) = \Omega t$. The resulting chip thickness consists of a static component $f_t \sin \phi_j$, where f_t is feed per revolution, which is due to rigid body motion of the cutter and a dynamic component $(n_{j-1} - n_j)$ caused by the vibrations of the tool at the present (n_j) and previous (n_{j-1}) tooth periods. Since the chip thickness is measured in radial direction (n), the instantaneous variable total chip thickness is expressed as:

$$h(\varphi_j) = (f_t \sin(\varphi_j) + n_{j-1} - n_j) g(\varphi_j) \quad (12)$$

where the switching function, $g(\varphi_j)$, is equal to one when the j^{th} tooth is engaged in the cut (i.e., between the cut start and exit angles) and zero otherwise and is expressed as:

$$g(\varphi_j) = \begin{cases} 1, & \text{when } \varphi_s \leq \varphi_j \leq \varphi_e \\ 0, & \text{when } \varphi_j < \varphi_s, \varphi_j > \varphi_e \end{cases} \quad (13)$$

where φ_s and φ_e are start and exit immersion angles of the cutter to and from the cut, respectively. As static part of the chip thickness ($f_t \sin \varphi_j$) has no effect on the dynamic chip load regeneration mechanism, Eq. (11) reduces to

$$h(\varphi_j) = (\Delta x \sin(\varphi_j) + \Delta y \cos(\varphi_j)) g(\varphi_j) \quad (14)$$

where

$$\Delta x = x(t) - x(t - \tau); \Delta y = y(t) - y(t - \tau); \tau = \frac{2\pi}{N_t \Omega} \quad (15)$$

$[x(t) \ y(t)]$ and $[x(t-\tau) \ y(t-\tau)]$ represent dynamic displacements of the cutter at the present and previous tooth periods and τ is the delay time or tooth passing period. The components of linear cutting force in tangential and radial directions ($F_{t,j}$ and $F_{r,j}$) acting on the tooth j is proportional to the axial depth of cut (b) and chip thickness $h(\varphi_j)$

$$F_{r,j}(\varphi) = K_r F_{t,j}(\varphi) = K_r K_t b h(\varphi_j) \quad (16)$$

$$F_{t,j}(\varphi) = K_t b h(\varphi_j) \quad (17)$$

where flute coefficients K_t and K_r are contributed by shearing in respectively tangential and normal directions. The projections of the tangential and normal force components onto the fixed (x and y) coordinate frame are

$$F_{x,j} = -F_{t,j} \cos \phi_j - F_{r,j} \sin \phi_j \quad (18)$$

$$F_{y,j} = +F_{t,j} \sin \phi_j - F_{r,j} \cos \phi_j \quad (19)$$

The closed-form expressions for cutting forces are computed by including the summation over all the teeth (flutes) to obtain the total forces as:

$$F_x(\varphi) = \sum_{j=1}^{N_t} F_{x,j}; F_y(\varphi) = \sum_{j=1}^{N_t} F_{y,j} \quad (20)$$

The x and y direction force expressions are arranged in matrix form

$$\begin{Bmatrix} F_x \\ F_y \end{Bmatrix} = \frac{1}{2} \mathbf{bK}_t \begin{bmatrix} a_{xx} & a_{xy} \\ a_{yx} & a_{yy} \end{bmatrix} \begin{Bmatrix} \Delta x \\ \Delta y \end{Bmatrix} = \frac{1}{2} \mathbf{bK}_t [A(t)] (\Delta(t)) \quad (21)$$

where the elements of matrix $[A]$ are the time varying directional dynamic force coefficients depends on the angular position of the cutter which can be expressed as:

$$a_{xx} = \sum_{j=1}^{N_t} -g(\varphi_j) [(\sin(2\varphi_j) + K_r(1 - \cos(2\varphi_j)))] \quad (22a)$$

$$a_{xy} = \sum_{j=1}^{N_t} -g(\varphi_j) [(1 + \cos(2\varphi_j)) + K_r(\sin(2\varphi_j))] \quad (22b)$$

$$a_{yx} = \sum_{j=1}^{N_t} g(\varphi_j) [(1 - \cos(2\varphi_j)) - K_r(\sin(2\varphi_j))] \quad (22c)$$

$$a_{yy} = \sum_{j=1}^{N_t} g(\varphi_j) [(\sin(2\varphi_j) - K_r(1 + \cos(2\varphi_j)))] \quad (22d)$$

These expressions are periodic with the tooth pitch:

$$\varphi_p = \frac{2\pi}{N_t} \text{ (rad) and tooth period } \tau = \frac{60}{\Omega N_t} \text{ (s). In general,}$$

the Fourier series expansion of the periodic term is used for the solution of the periodic systems. In stability analysis, the single chatter frequency is usually dominated and the higher harmonics in solution may not be required. Thus, the average term in Fourier series expansion of $[A(t)]$ is included to reduce the Eq.(20) to the following form:

$$\{F(t)\} = \frac{1}{2} \mathbf{bK}_t [A_0] \{\Delta(t)\} \quad (23)$$

where $[A_0]$ consists of four directional orientation factors defined as follows:

$$\alpha_{xx} = \frac{1}{2} [(\cos(2\varphi) - 2K_r\varphi + K_r \sin(2\varphi))]_{\varphi_s}^{\varphi_e} \quad (24a)$$

$$\alpha_{xy} = \frac{1}{2} [(-\sin(2\varphi) - 2\varphi + K_r \cos(2\varphi))]_{\varphi_s}^{\varphi_e} \quad (24b)$$

$$\alpha_{yx} = \frac{1}{2} [(-\sin(2\varphi) + 2\varphi + K_r \cos(2\varphi))]_{\varphi_s}^{\varphi_e} \quad (24c)$$

$$\alpha_{yy} = \frac{1}{2} [(-\cos(2\varphi) - 2K_r\varphi - K_r \sin(2\varphi))]_{\varphi_s}^{\varphi_e} \quad (24d)$$

3.1. Machining Stability

By substituting the response and delay terms in Eq. (22), the following expression is obtained.

$$\{F\} e^{i\omega_c t} = \frac{1}{2} \mathbf{bK}_t [A_0] (1 - e^{-i\omega_c \tau}) [G(i\omega_c)] \{F\} e^{i\omega_c t} \quad (25)$$

where $\{F\}$ represents the amplitude of dynamic milling force vector $\{F(t)\}$ and the transfer function matrix is given as:

$$[G(i\omega_c)] = \begin{bmatrix} G_{xx} & G_{xy} \\ G_{yx} & G_{yy} \end{bmatrix} \quad (26)$$

Here the terms are computed as summation of the cutter and work piece transfer function components. The characteristic equation of the closed loop dynamic milling system is finally expressed as:

$$\det \left([I] - \frac{1}{2} \mathbf{bK}_t (1 - e^{-i\omega_c \tau}) [A_0] [G(i\omega_c)] \right) = 0 \quad (27)$$

where the product $[A_0][G(i\omega_c)]$ gives the oriented frequency response function $[G_0]$. A new variable, Λ is now introduced as

$$\Lambda = -\frac{N_t}{4\pi} \mathbf{bK}_t (1 - e^{-i\omega_c \tau}) \quad (28)$$

So that the characteristic equation can be rewritten as

$$\det([I] + \Lambda[FRF_{or}]) = 0 \quad (29)$$

The eigenvalue of the above equation can easily be solved for a given chatter frequency ω_c , static cutting factors (K_t, K_r), radial immersion angles (φ_s and φ_e) and frequency response function of the structure. By using,

$$\kappa = \frac{\Lambda_{Im}}{\Lambda_{Re}} = \frac{\sin \omega_c \tau}{1 - \cos \omega_c \tau} \quad (30)$$

the expression for the stability limit is obtained as:

$$b_{lim} = -\frac{2\pi}{N_t K_t} \quad (31)$$

The corresponding frequency dependent spindle speeds are determined by first writing the phase shift in the surface undulations between subsequent tooth passages, $\varepsilon = \pi - 2\psi$ where $\psi = \tan^{-1}(\kappa)$. The tooth passing

periods are next expressed as $\tau = \frac{1}{\omega_c}(\varepsilon + j2\pi)$, where $j=0, 1, 2, \dots$ refers to the integer number of waves between the teeth and incrementing j leads to the individual lobes.

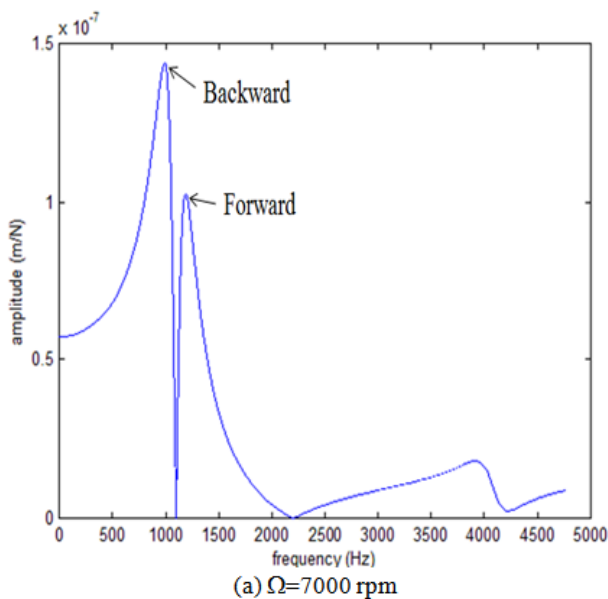
Finally the spindle speeds are obtained from

$$\Omega = \frac{60}{N_t \tau} \text{ (rpm)} \quad (32)$$

In present context, an average stable depth of cut is computed in order to study the effect of spindle parameters on stability. It is defined according to the following equation:

$$a = \frac{\int_0^{N_{max}} b_{lim} dN}{\int_0^{N_{max}} dN} \quad (33)$$

where N_{max} refers to the maximum speed limit in stability lobe diagram.



4. Results and Discussions

The parameters of the finite element model of the spindle are illustrated in Table 1. Except the element-1 (silicon carbide tool), all elements have material properties of steel. Densities and shear modulus are obtained from tables.

Table 1. Parameters of the finite element model of the spindle

| Parameter | Element of the spindle | | | | | |
|-------------|------------------------|--------|--------|--------|--------|--------|
| | #1 | #2 | #3 | #4 | #5 | #6 |
| Length (mm) | 45 | 40 | 50 | 20 | 200 | 20 |
| dia. (mm) | 19 | 74.5 | 40 | 80 | 80 | 80 |
| E (Pa) | 4.5e11 | 2.1e11 | 2.1e11 | 2.1e11 | 2.1e11 | 2.1e11 |

Computer program is developed in MATLAB to analyze the spindle system. The assembling of matrices and static condensation procedure for eliminating the rotational degrees of freedom are implemented in a single program. Campbell diagram is plotted for the beam model as shown in Figure 3. Using undamped natural frequencies, the coefficients of Rayleigh's damping α and β are obtained as 17.32 and $3.87e-6$ respectively for 1% damping ratio.

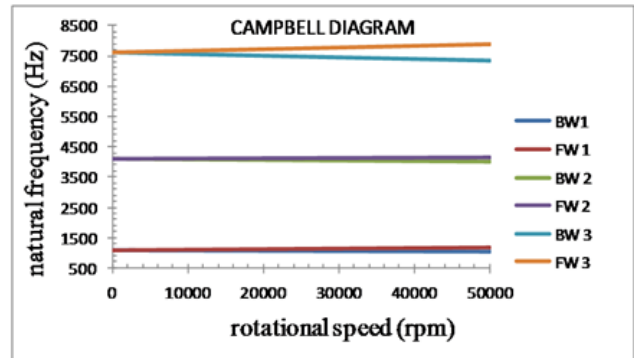


Figure 3. First three whirl frequencies of spindle rotor

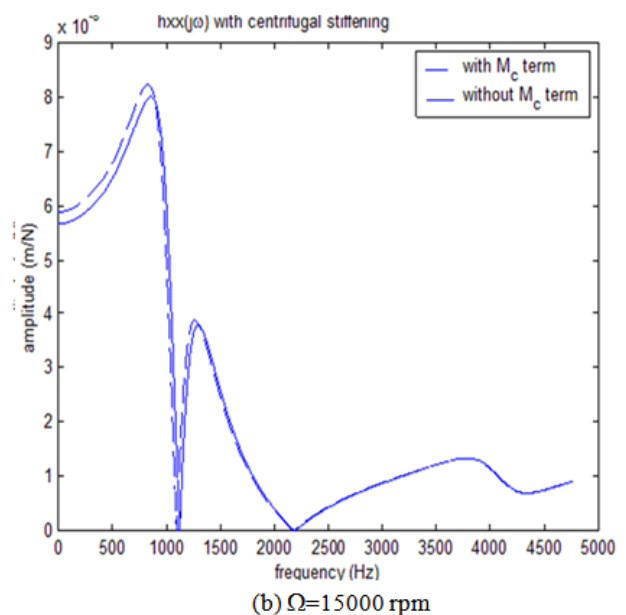


Figure 4. Tool tip frequency response of spindle by considering static radial stiffness

The forward and backward whirl modes are obvious due to the gyroscopic effect at first three natural frequencies 927.8 Hz, 4079.1 Hz and 7590.57 Hz respectively. In order illustrate the centrifugal stiffening effect and bearing dynamics, direct frequency response function at the tool tip $h_{xx}(j\omega)$ is obtained at different spindle speeds (Ω). Figure 4 depicts the FRF without considering viscous damping for the spindle mounted on bearings at two different speeds. The effect of centrifugal stiffening is observed at higher speeds only as seen in Figure 4b.

Unlike direct FRF, the cross FRF is a smooth curve without showing backward (BW) and forward (FW) whirl modes as seen from the Figure 5 obtained at 15000 rpm.

The effect of viscous damping on the tool tip FRF is shown at 12000 rpm as shown in Figure 6. It is seen that damping influences whirl modes considerably.

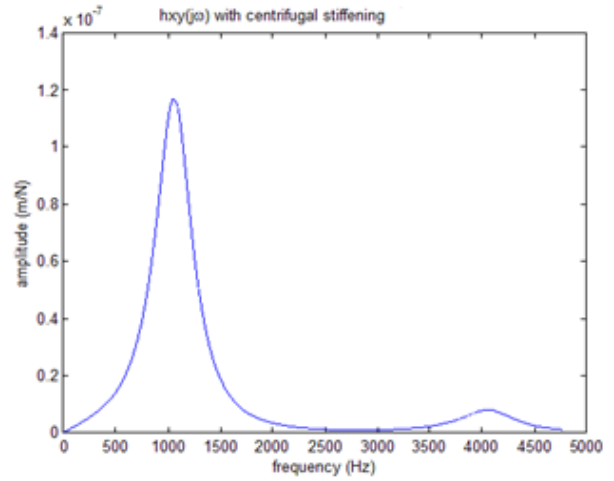
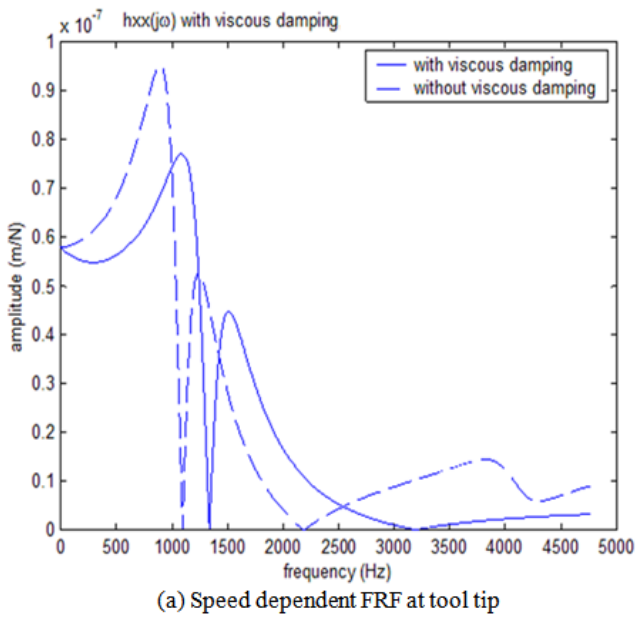
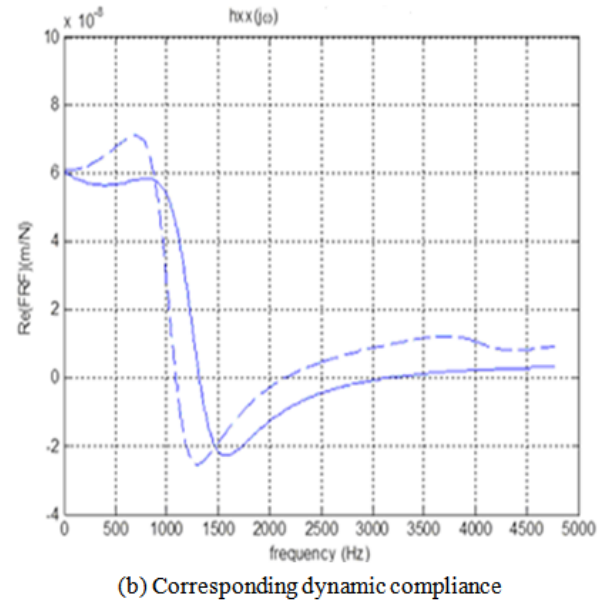


Figure 5. Cross frequency response at 15000 rpm

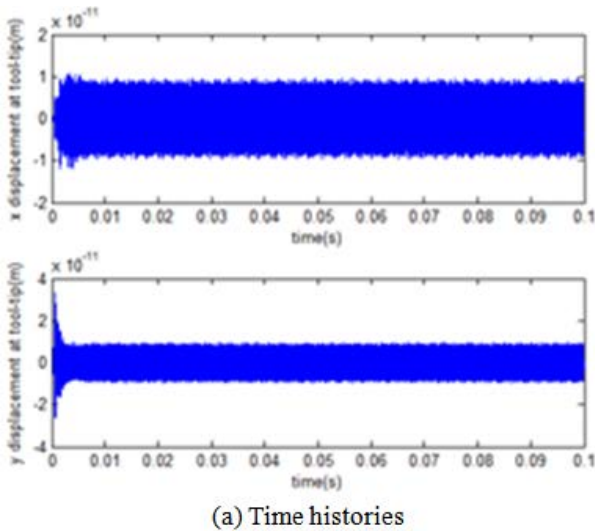


(a) Speed dependent FRF at tool tip

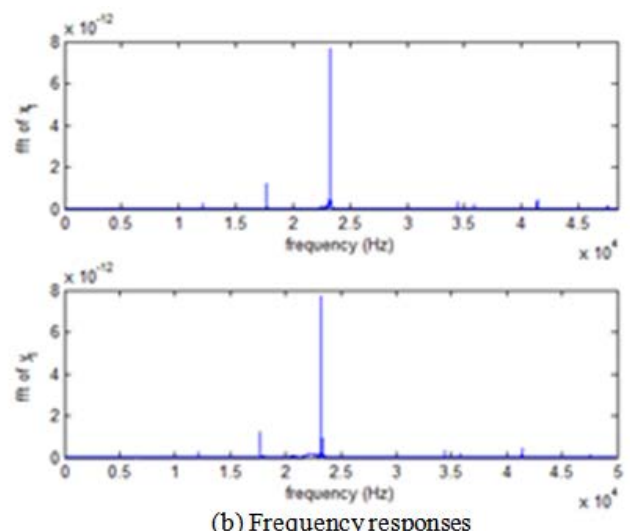


(b) Corresponding dynamic compliance

Figure 6. Effect of viscous damping at a speed 12000 rpm



(a) Time histories



(b) Frequency responses

Figure 7. Transient response solution to bearing contact forces

For studying the effect of bearing contact forces, the solution is obtained as a transient analysis problem, first in time domain and then the frequency spectrum is derived

from fast Fourier transformation (FFT) algorithm. The reduced coupled differential equations (fourteen in number) are solved explicitly, by using Runge Kutta time

marching method. Figure 7 shows the time histories and corresponding FFT diagram at the tool-tip node corresponding to the following bearing parameters: inner radius $r=20\text{mm}$, outer radius $R=40\text{ mm}$, number of ball $N_b=9$, $k_{b1}=k_{b2}=13.34\times 10^9\text{ N/m}^{3/2}$, clearance $\delta=-0.05\text{ }\mu\text{m}$ (in considering practical conditions, the interference fit generally adapted to chatter problems where negative clearance is justified).

It is clearly observed from frequency responses that the natural frequencies of the spindle have been affected by the bearing contact forces.

4.1. Three Dimensional Spindle Model

A solid model is developed as an assemblage of angular contact ball bearings at the front and rear positions with the spindle-tool unit as shown in the Figure 8. To introduce the boundary conditions, the outer races of the front and rear bearings is fixed while the inner races are allowed to rotate with the spindle tool unit.

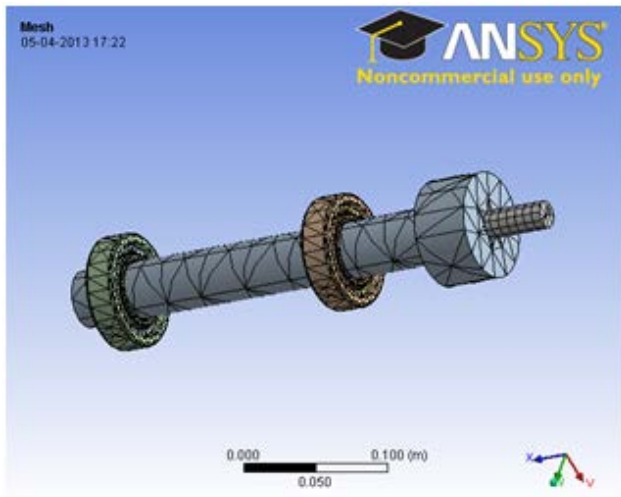


Figure 8. Solid mesh model of spindle bearing system

Using 8-node SOLID 187 elements, the spindle shaft and tool holder as well as cutting tool are discretized with the same material properties as considered for one-dimensional model. The modal analysis of static spindle system revealed the first few natural frequencies as depicted in Table 2.

Table 2. Natural Frequencies from Modal Analysis

| Mode | Frequency (Hz) |
|------|----------------|
| 1 | 921.765 |
| 2 | 923.925 |
| 3 | 2427.89 |
| 4 | 4584.65 |
| 5 | 4600.86 |
| 6 | 4875.17 |
| 7 | 4884.64 |
| 8 | 5025.28 |
| 9 | 6794.56 |
| 10 | 6807.61 |

It is observed that these frequencies have considerable agreement with the Timoshenko beam theory. Harmonic response analysis is carried to predict the sustained

dynamic behavior of spindle bearing system and by this we can observe the peak responses as shown in Figure 9.

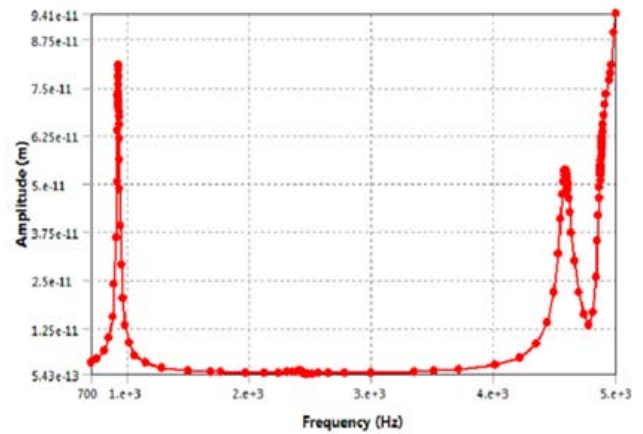


Figure 9. Harmonic response of spindle bearing system

The phase response has also been plotted as shown in Figure 10 in conjunction with the harmonic plots to show a response over a range of phase angles, so that it can determine how much a response lags behind the applied load.

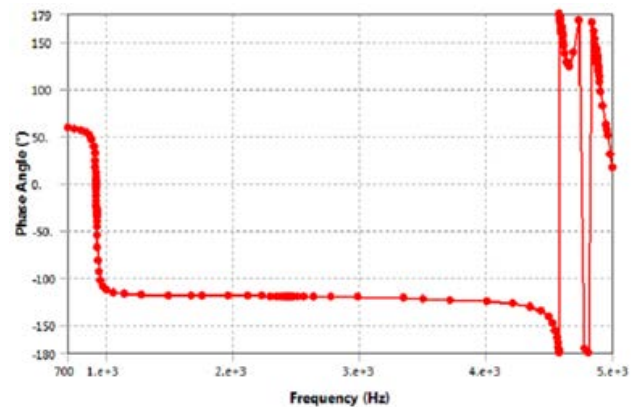


Figure 10. Phase response of the spindle bearing system

4.1.1. Prediction of Stability Charts Related to the Design Variables

The force variation excites the system dynamics and causes vibrations which lead to subsequent changes in the chip thickness. This feedback mechanism can lead to unstable behavior, exhibited as self-excited vibrations or chatter. The phase difference between engagements depends on the spindle speed and axial depth of cut acts as the feedback system gain. Stability information can be presented using different input parameters such as axial depth, spindle speed and radial depth. Often, the stability lobe boundary is predicted in the spindle speed and axial depth domain. The graphical representation of this relationship is a boundary between stable and unstable cutting zones (displayed as a function of spindle speed and axial depth). It is referred to as a stability lobe diagram. The main advantage of the chatter prediction through the stability lobes diagram is the metal removal rate maximization, at the same time avoiding the adverse effects of chatter vibrations like the poor surface finish, noise and breakage of tools. Any operating point above the boundary is considered unstable, while all the points below are considered stable. In this paper, direction

dynamics are considered as $K_x=K_y=2.1 \times 10^8$ N/m. Also the tool diameter=19mm, helix angle of tooth (β) =68°, average specific cutting pressure of low-carbon steel alloy $K_s=2250$ N/mm², the number of teeth=4 and damping ratios used are: $\xi_x = \xi_y = 0.01$. The stability regions are

plotted for the up-milling process at different depths of radial immersions as shown in Figure 11 using the first two modal frequencies obtained from the finite element analysis. Obviously, the limiting depth of cut decreases with increase of radial immersion.

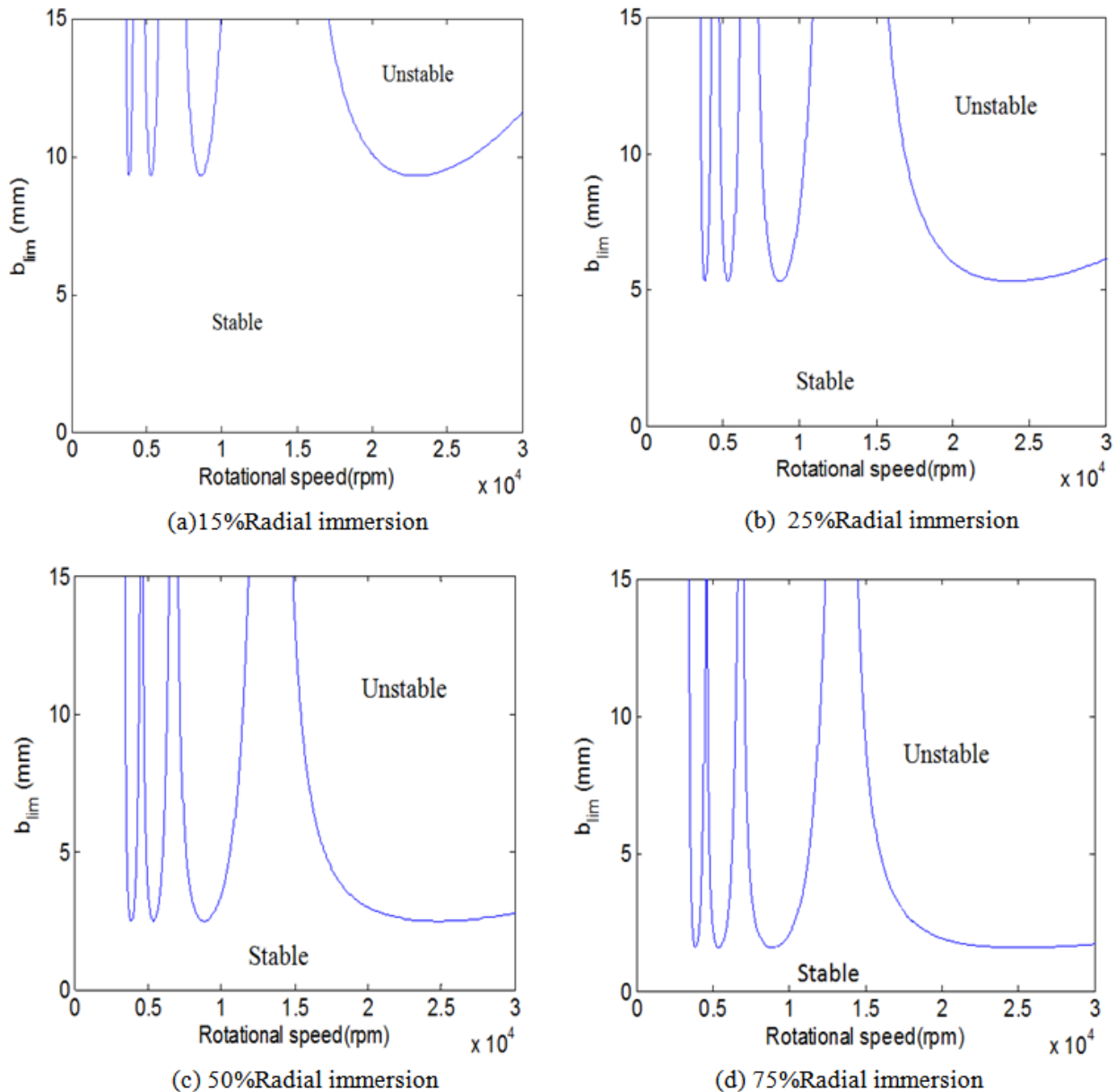


Figure 11. Stability lobe plots for different percentages of radial immersion

In order to design an optimized spindle for effective utilization of cutting processes many performance parameters can be selected as objectives, such as minimum weight, highest basic frequency, maximum dynamic stiffness, depth of cut and so on. Among all of these parameters, the maximum dynamic stiffness and average stable depth of cut are directly related to chatter vibration, which are the most important issues to be considered. There are significant number of important design parameters related to these issues such as the dimensions of spindle shaft and its housing and bearing locations, preload of the bearings, tool over hang and helix angle of the cutting tool. In the present work, slot milling for different conditions of the bearing span, tool over hang and helix angle of the cutting tool is considered and effect of these parameters on stable depth of cut are plotted.

Figure 12(a)-Figure 12(c) shows the effect of tool overhang on the dynamics of cutting. It is observed that when an increase in the length of tool overhangs there is an decrease of average stable depth of cut. The overhang length has the most influence in changing the milling dynamics of the system.

Figure 13(a)-Figure 13(c) shows the effect of bearing span on the stability of the spindle system. It is observed that when there is an increase in the bearing span ratio the second mode of vibration came into existence which critically influences the dynamic stability of the system and it forms the competing lobes inside the original lobes and axial depth of cut increases for a bearing span of 500mm as shown in Figure 13(b).

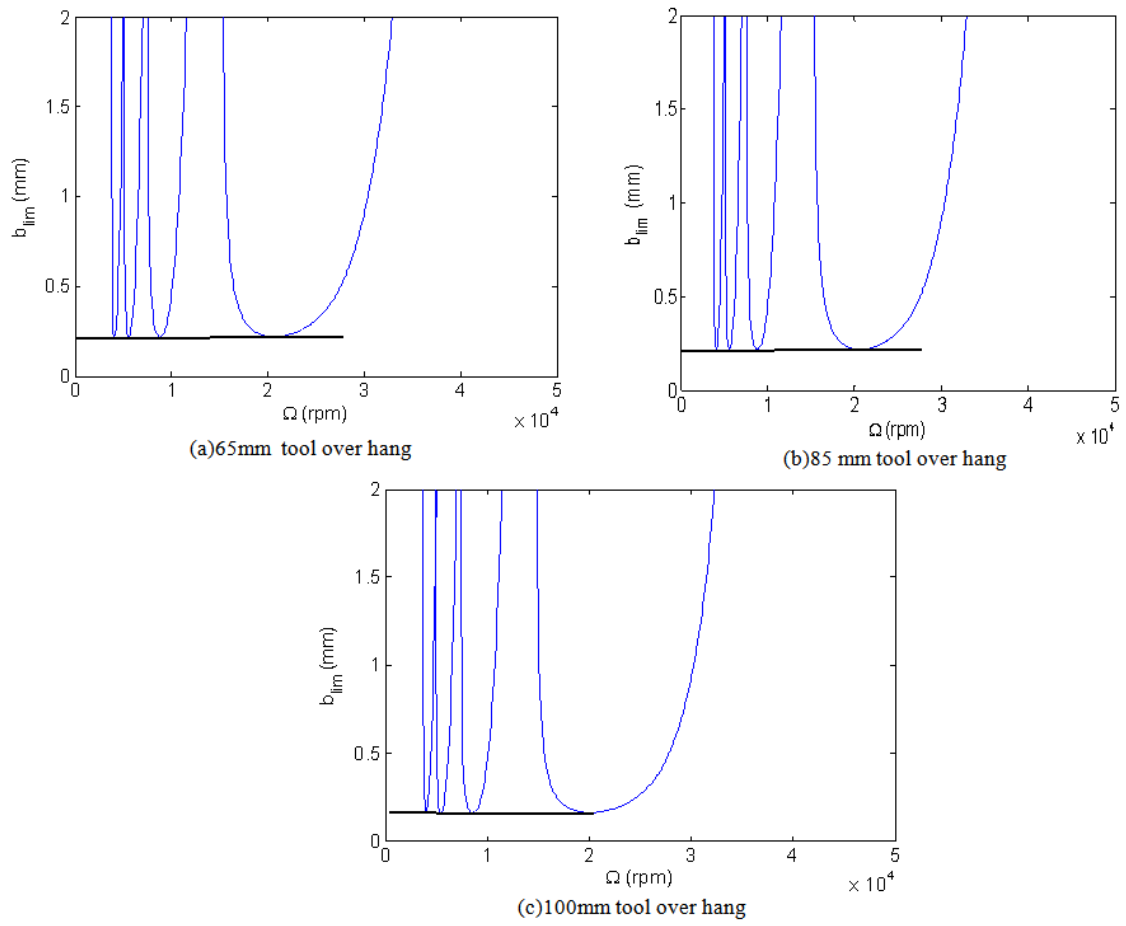


Figure 12. Effect of tool overhang on stability

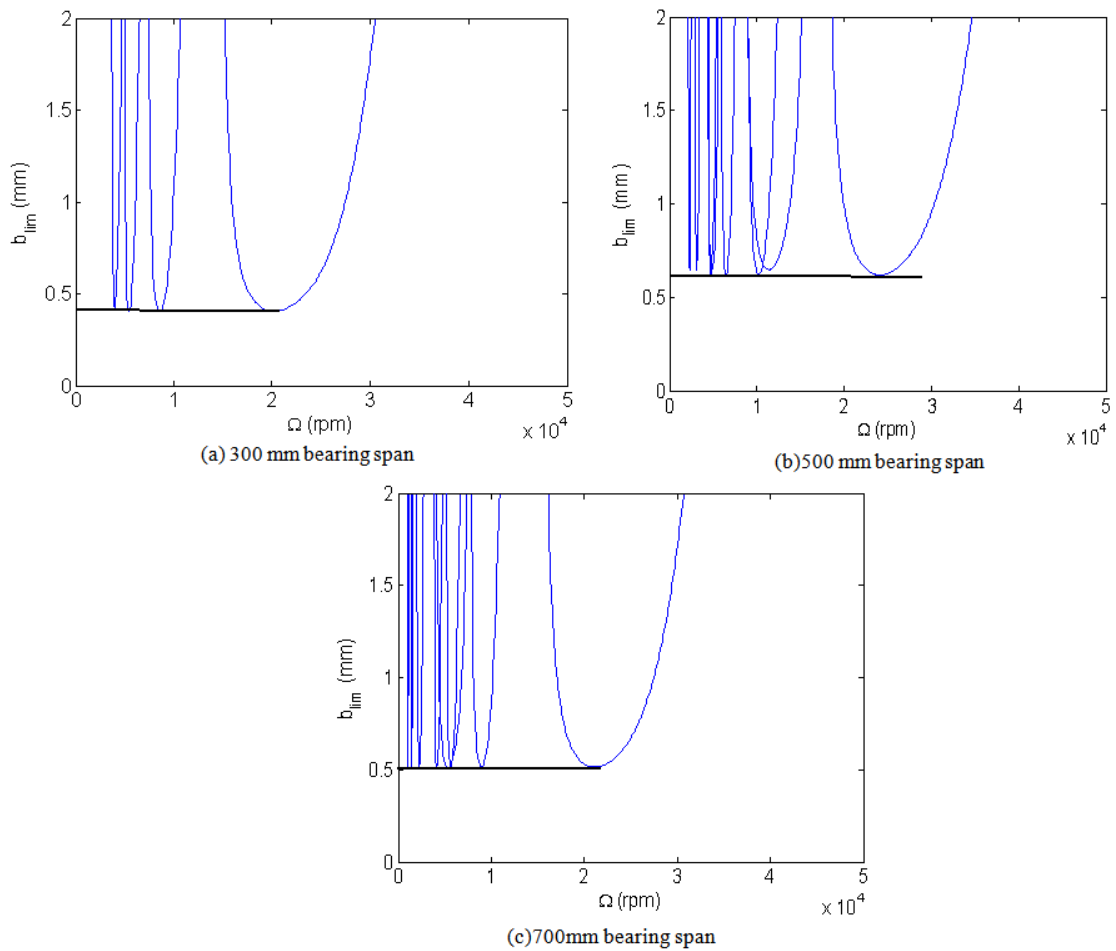


Figure 13. Effect of bearing span on stability

Figure 14(a)-Figure 14(c) gives the various trends of helix angle on the dynamics of the cutting process. It is

identified from the plots that high helix angle is needed to increase the depth of cut.

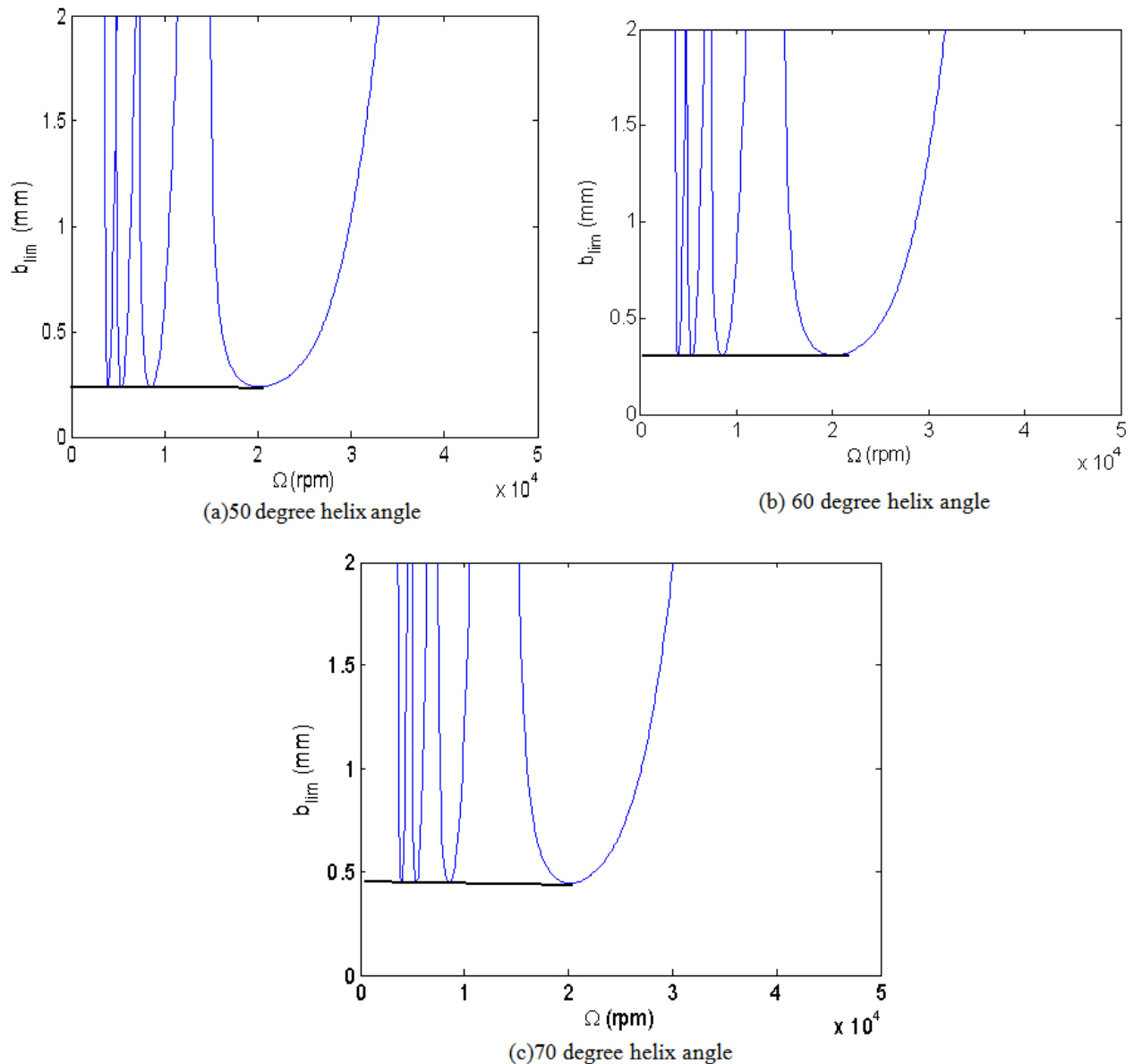


Figure 14. Effect of helix angle on stability

It was confirmed from results that the variation of the helix angle of the tool has profound influence on the stability. The average stable depth of cut increases when there is an enhance in helix angle of the cutting tool.

4.1.2. Prediction of Cutting Forces

In this paper, a predictive time domain model is presented for the simulation and analysis of the dynamic cutting process and chatter vibration in milling. The cutting forces in both the x and y directions are determined by the input data of the work piece material, the tool geometry and the cutting conditions. The instantaneous undeformed chip thickness is modeled to include the dynamic modulations caused by the tool vibrations so that the dynamic regeneration effect was taken into account. Time-domain simulation gives the local force and vibration information for the selected cutting conditions. The simulation applies numerical integration to solve the time delayed differential equations of motion and includes the nonlinearity that occurs if tooth

leaves the cut. This simulation gives the information about the instantaneous chip thickness and it is determined using the vibration of the current and the previous teeth at the selected tooth angle. The cutting force is calculated and it is used to find the new displacements. The instantaneous chip thickness depends on the nominal-tooth angle dependent-chip thickness, the current normal direction vibration and the vibration of the previous tooth at the same angle. For the simulation time marching technique using Euler integration, divides the angle of cut is into a discrete number of steps. At each small time step, dt increment the cutter angle by the corresponding small angle, $d\phi$. Once the chip thickness is computed, the tangential component of the force in current step is determined and these forces are then resolved and summed for the milling cutting forces in x and y directions. The process continues until the cutter has completed one revolution, from which the force variation for one cycle of the cutting will be simulated as shown in Figure 15(a)-Figure 15(c).

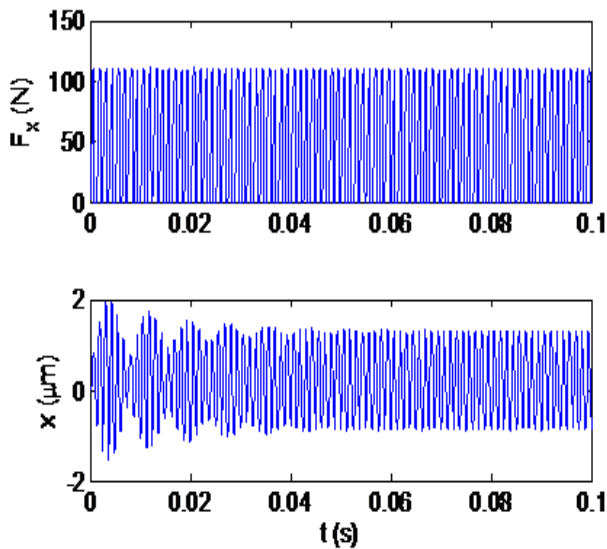


Figure 15a. Simulated cutting forces and displacement along X direction at an axial depth of 5mm

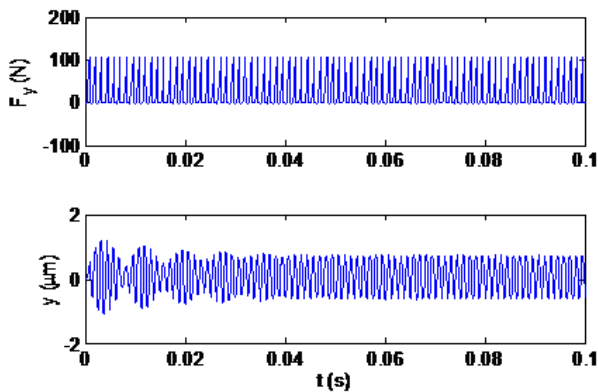


Figure 15b. Simulated cutting forces and displacement along Y direction at an axial depth of 5mm

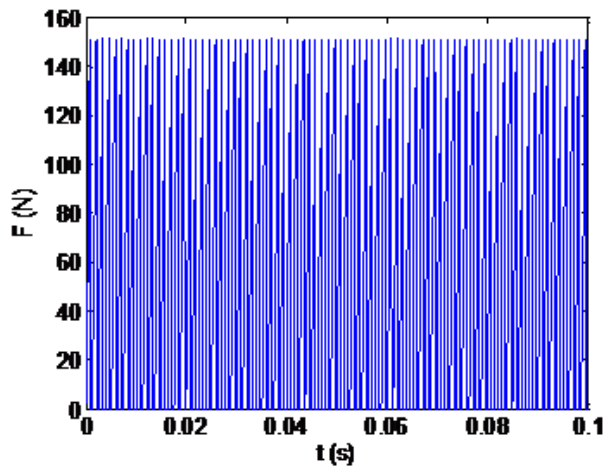


Figure 15c. Simulation results for the resultant cutting force (F)

5. Conclusions

This paper has illustrated speed varying spindle dynamics using frequency responses at the tool tip. A model was considered for illustration and analyzed using finite element analysis by considering the effect of shear deformation and rotary inertia of spindle shaft. The

vibration characteristics of the system were verified using a three-dimensional model of spindle bearing system by conducting modal and harmonic analysis. Based on the formulation of dynamic milling with regeneration in the chip thickness, the stability lobes are plotted. Parametric studies were conducted by considering the different values of bearing span, tool overhang and cutting angle and studied their influence on average stable depth of cut. Based on the above parametric studies it was clearly observed that with the enhancement of bearing span competing lobes are formed inside the lobes and the helix angle of the cutting tool has wide influence over the average stable depth of cut.

References

- [1] Altintas, Y. and Budak, E., "Analytical prediction of stability lobes in milling," *Annals of the CIRP*, 44, 357-362. 1995.
- [2] Schmitz, T.L., Davies, M.A., Medicus, K. and Snyder, J., "Improving high-speed machining material removal rates by rapid dynamic analysis," *Annals of the CIRP*, 50, 263-268. 2001.
- [3] Schmitz, T.L., Ziegert, J.C., Stanislaus, C., "A method for predicting chatter stability for systems with speed-dependent spindle dynamics," *Trans. North Amer. Manuf. Res. Institution of SME*, 32, 17-24. 2004.
- [4] Schmitz, T.L. and Duncan, G.S., "Three-component receptance coupling substructure analysis for tool point dynamics prediction," *J Manuf Sci Eng*, 127, 781-791. 2005.
- [5] Cheng, C.H., Schmitz, T.L. and Duncan, G.S., "Rotating tool point frequency response prediction using RCSA," *Machining Science and Technology*, 11, 433-446. 2007.
- [6] Jun, Z., Tony, S., Wanhua, Z. and Bingheng, L.U., "Receptance coupling for tool point dynamics prediction on machine tools," *Chinese J. Mech. Engg.*, 24, 1-6. 2011.
- [7] Kumar, U.V. and Schmitz, T.L., "Spindle dynamics identification for Receptance Coupling Substructure Analysis," *Precision Engineering*, 36, 435-443. 2012.
- [8] Erturk, A., Budak, E. and Ozguven, H.N., "Selection of design and operational parameters in spindle-holder-tool assemblies for maximum chatter stability by using a new analytical model," *Int. J. Machine Tools & Manf.*, 47, 1401-1409. 2007.
- [9] Faassen, R.P.H., Wouw, N.V., Oosterling, J.A.J. and Ijmeijer, H.N., "Prediction of regenerative chatter by modelling and analysis of high-speed milling," *Int. J. Machine Tools & Manf.*, 43, 1437-1446. 2003.
- [10] Abele, E. and Fiedler, U., "Creating stability lobe diagrams during milling," *Annals of the CIRP*, 53, 309-312. 2004.
- [11] Zaghbani, I. and Songmene, V., "Estimation of machine-tool dynamic parameters during machining operation through operational modal analysis," *Int. J. Machine Tools & Manf.*, 49, 947-957. 2009.
- [12] Chen, C.H. and Wang, K.W., "An integrated approach toward the dynamic analysis of high-speed spindles: Part-2. Dynamics under moving end load," *J. Vibration and Acous. Trans. ASME*, 116, 514-522. 1994.
- [13] Tian, J.F. and Hutton, S.G., "Chatter instability in milling systems with flexible rotating spindles—a new theoretical approach," *J. Manuf. Sci. and Engg. Trans. ASME*, 123, 1-9. 2001.
- [14] Xiong, G.L., Yi, J.M., Zeng, C., Guo, H.K. and Li, L.X., "Study of the gyroscopic effect of the spindle on the stability characteristics of the milling system," *Journal of Materials Processing Technology*, 138, 379-384. 2003.
- [15] Movahhedy, M.R. and Mosaddegh, P., "Prediction of chatter in high speed milling including gyroscopic effects," *Int. J. Machine Tools & Manuf.*, 46, 996-1001. 2006.
- [16] Gagnol, V., Bougarrou, B.C., Ray, P. and Barra, C., "Stability based spindle design optimization," *J. Man. Sci. Eng. Trans. ASME*, 129, 407-415. 2007.
- [17] Jiang, S. and Zheng, S., "A modeling approach for analysis and improvement of spindle-drawbar-bearing assembly dynamics," *Int. J. Mach. Tools & Manuf.*, 50, 131-142. 2010.

- [18] Gao, S.H., Meng, G. and Long, X.H., "Stability prediction in high-speed milling including the thermal preload effects of bearing," *J. Process Mech. Engg. Proc. IMechE*, 224, 11-22. 2010.
- [19] Cao, H., Holkup, T. and Altintas, Y., "A comparative study on the dynamics of high speed spindles with respect to different preload mechanisms," *Int J Adv Manuf Technol*, 57, 871-883. 2011.
- [20] Gagnol, V., Le, T.P. and Ray, P., "Modal identification of spindle-tool unit in high-speed machining," *Mech. Sys. Sig. Proc.*, 25, 238-239. 2011.
- [21] Cao, H., Li, B. and He, Z., "Chatter stability of milling with speed-varying dynamics of spindles," *Int.J.Mach.Tools and Manuf.*, 52, 50-58. 2012.
- [22] Cao, Y. and Altintas, Y., "A general method for modeling of spindle bearing system," *J. Mech. Design, Trans. ASME*, 126, 1089-1104. 2004.
- [23] Rantatalo, M., Aidanpaa, J.O., Goransson, B. and Norman, P., "Milling machine spindle analysis using FEM and non-contact spindle excitation and response measurement," *Int. J. Machine Tools & Manuf.*, 47, 1034-1045. 2007.
- [24] Nelson, H.D., "A finite rotating shaft element using Timoshenko beam theory," *J. of machine design*, 102, 793-803. 1980.
- [25] Liu, D., Zhang, H., Tao, Z. and Su, Y., "Finite element analysis of high-speed motorized spindle based on ANSYS," *The open Mechanical Engineering Journal*, 5, 1-10. 2011.
- [26] Quo, Q., Sun, Y. and Jiang, Y., "On the accurate calculation of milling stability limits using third-order full-discretization method," *International Journal of Machine Tools & Manufacture*, 62, 61-66. 2012.